Fuel supply system to DOC by nanopore-ceramic tube and measurement of fuel evaporation rate

by

Kazuhiro YAMAMOTO, Kenju YOSHIZAWA
Dep. Mechanical Systems Engineering, Nagoya University
Furo-cho, Chikusa-ku, Nagoya, Aichi 464-8603, JAPAN

Corresponding author: Kazuhiro Yamamoto
Dep. Mechanical Systems Engineering
Faculty of Engineering
Nagoya University
Furo-cho, Chikusa-ku, Nagoya, Aichi 464-8603, Japan
Tel: (+81)-52-789-4471, Fax: (+81)-52-789-4471
E-mail address: kazuhiro@mech.nagoya-u.ac.jp

Keywords: Diesel soot; Oxidation; Porous media; Fuel evaporation, Burning velocity

Fuel supply system to DOC by nanopore-ceramic tube and measurement of fuel evaporation rate

by

Kazuhiro YAMAMOTO, Kenju YOSHIZAWA
Dep. Mechanical Systems Engineering, Nagoya University
Furo-cho, Chikusa-ku, Nagoya, Aichi 464-8603, JAPAN

ABSTRACT

When the deposited particles in DPF is oxidized, diesel fuel is injected to the diesel oxidation catalyst (DOC) for increasing the exhaust gas temperature. It is called a secondary fuel injection. However, it is difficult to form the uniform fuel mixture. If there is high fuel concentration region, hot spots and/or coking at the catalyst inlet face, leading to the potential damage of the catalyst. Also, the fuel must be completely evaporated to avoid the emission of harmful hydrocarbons in the outer atmosphere. Non-uniform fuel supply across the catalyst inlet face may cause incomplete fuel oxidation over the DOC. Thus, we may need an alternative approach for fuel supply system in the exhaust line. In this study, we have tested a fuel supply system to DOC using nanopore-ceramic tube. The fuel is uniformly vaporized on the surface of the tube filled with the diesel fuel, which automatically flows towards the DOC. Since we could not measure the vaporized gaseous component by an electrical low pressure impactor called ELPI+, the evaporation rate was evaluated in terms of the burning velocity of the premixed flame on a Bunsen burner. It was confirmed that most of water vaporized from the ceramic tube was gaseous water vapor. As the pore size of the tube was larger, the maximum evaporation rate increased. When the tube length or the tube outer diameter was larger, the fuel evaporation was enlarged due to the larger surface area of the fuel evaporation.

1. Introduction

In order to deal with global warming, the Paris Agreement has been passed at the twenty-first session of the Conference of the Parties (COP 21) in 2015 [1]. Its implementation needs us to take a variety of economic and social actions on a global scale. Each country is supposed to submit an appropriate plan suitable for climate change, which is known as nationally determined contributions (NDCs). Therefore, for the reduction of greenhouse gas emissions including CO_2, several countries will try to expand use of electric vehicles (EVs), instead of vehicles with so-called internal combustion engines operated by fossil fuels. For example, the U.K. will quit selling new diesel and gasoline cars and vans from 2030. However, in the countries all over the world, it is difficult to supply more electricity for increasing demands for EVs under rapid economic growth especially in developing counties. Then, we may still need internal combustion engines in next several tens of years.

It is well-known that diesel engines have better fuel conversion efficiency than that of gasoline engines

12 [2,3], but they emit more particulate matters (PMs), which is the cause of human carcinogens [4,5]. Currently, in

13 EUs, US and Japan, much stricter exhaust emission standards have been set for reduction of diesel soot emission

14 [6,7]. As for the exhaust after-treatment system, a diesel particulate filter (DPF) [8-11], as well as a gasoline

15 particulate filter (GPF) [12-15], is widely used. However, during filtration for diesel soot, more deposited

16 particulates surely induce the pressure across the filter to increase, causing a decrease in engine output and a

17 subsequent worsening of fuel efficiency [16-18]. To avoid this situation, the filter must be cleaned by the well-

18 known filter regeneration process, corresponding to an incineration step to oxidize the deposited soot. The filter

19 inlet temperature must be higher than 550 ˚C for the soot oxidation [16]. Generally, more diesel fuel is injected

20 into the exhaust line at the location upstream of a diesel oxidation catalyst (DOC), where the diesel fuel is

21 catalytically reacted with an exothermic oxidation. Resultantly, the exhaust gas temperature is increased, and the

22 deposited particulates in DPF are removed. Thus, the DOC is used as the heat-up catalyst for temperature increase.

It is expected that NO_2 is formed by the DOC, so that the deposited soot is efficiently oxidized [19-22].

There are two ways for fuel supply to the DOC in the diesel exhaust gas line. One is to inject more diesel fuel in the engine cylinder after the main combustion is apparently ended. It corresponds to an additional fuel post-injection [23,24]. In this case, unburned fuel passes through the exhaust valve and flows downstream to the DOC. However, a part of unburned fuel could remain in the engine cylinder, by which the engine oil is diluted, because some fuel passes through the gap between the piston and the engine wall, causing the engine trouble. The other is to supply the diesel fuel by using an additional injector on the way of the exhaust pipe. The location of this fuel injector is set between the engine exhaust manifold and the DOC. It is called a secondary fuel injection [25,26]. However, it is difficult to form the uniform fuel mixture. If there is high fuel concentration region, hot spots and/or coking at the catalyst inlet face, leading to the potential damage of the catalyst. Also, the fuel must be completely evaporated and oxidized to avoid the emission of harmful hydrocarbons in the outer atmosphere.

Non-uniform fuel supply across the catalyst inlet face may cause incomplete fuel oxidation over the DOC, as well as non-uniform DOC outlet temperature with worsening the catalyst durability [27,28]. Thus, instead for both fuel supply systems, we may need an alternative approach.

In this study, we proposed a fuel supply system to the DOC for the filter regeneration. The diesel fuel is uniformly vaporized on the surface of the nanopore-ceramic tube, which automatically flows towards the DOC. Here, we measured the fuel evaporation rate though this porous tube by using an electrical low pressure impactor, called ELPI+ produced by Dekati Ltd. [29,30]. This device was used to detect particles in the range from 6 nm to 10 μm. Also, a method was tested to estimate the evaporation rate by the variation of the burning velocity of a premixed flame on a Bunsen burner.

2. Experimental setup

45 *2.1. Porous ceramic tube*

46 Figure 1 shows a nanopore-ceramic tube tested in the experiment. The inside of each ceramic tube was

47 a hollow cylinder with many nanopores on the tube surface. We used ceramic tubes with lengths 100, 200, and

48 280 mm and external diameters 10 mm (internal diameter: 6.9 mm) and 12 mm (internal diameter: 9 mm). To

49 change the evaporation characteristics, ceramic tubes with average pore diameters of 150, 500, and 1300 nm

50 were tested. Later, a summary of these dimensions are shown in Table 1 in Section 3.1. In the preparatory

51 experiment, water was used instead of diesel fuel. Before the evaporation experiments, the porous ceramic tubes

52 were deeply doped in the container filled with diesel fuel or water.

53

54 *2.2. Experimental method*

55 To measure the evaporation rate, the electrical low pressure impactor (ELPI+) was used. It can measure

the size distribution and number concentration of particles in 14 size fractions in the range from 6 nm to 10 μm at a maximum of 10 Hz. Figure 2 shows a schematic diagram of the measurement system. Each porous ceramic tube filled with water or diesel fuel was placed inside a tubular furnace with a temperature controller [16]. Then, the ceramic tube was heated to set a preset temperature of the mimic exhaust gas, so that the water or the diesel fuel impregnated in the tube was evaporated.

Next, we describe the method for the measurement of the amount of evaporated diesel fuel (water). Figure 3 shows a schematic diagram in this experiment. A premixed flame of gaseous fuel (not diesel fuel) and air was first formed on a burner used for forming the stable laminar flame. For the gaseous fuel of the premixed flame, methane was used. When diesel fuel or water was added in the flow line, the burning velocity of the premixed mixture was changed. Therefore, the amount of evaporated diesel fuel (water) could be estimated by the change of the burning velocity.

Here, we explain how to obtain the burning velocity experimentally. If the flow velocity of the mixture is slow enough, a laminar premixed flame is expected to be formed. Figure 4 shows the so-called Bunsen burner, where the corn-shaped stable flame is formed on the burner. The premixed flame tends to propagate toward the unburned mixture, it has a unique burning velocity. According to Fig. 4, the flame is inclined to the vertical line, and the burning velocity is simply obtained by the exit velocity of the mixture (U) and the half angle of the flame corn (θ), because the flame is propagated at the angle of θ to the inflow direction of the premixed mixture. In other words, the velocity component perpendicular to the flame front is balanced with the flame propagation velocity. It corresponds to the laminar burning velocity denoted as S_L, which is given by Eq. (1).

$$S_L = \mathrm{U} \sin\theta \quad (1)$$

In experiments, the flame was photographed using a digital camera to obtain the angle θ for the estimation of S_L. As shown in Fig. 4, the ceramic tube was installed in the flow line of the primary air, whose flow rate was 54

78 L/min. The flow rate of the secondary air which was mixed with methane was set at 8.2 L/min. The flow rate of

79 methane was 6.5 L/min, and the total equivalence ratio of the whole mixture was 1.0. In this case, the flow

80 velocity at the burner exit was 2 m/s, which was much larger than the burning velocity of the mixture, in order to

81 prevent the flash back of the premixed flame for the experimental safety. In the preliminary experiment, instead

82 of diesel fuel, water was used, because it was easy to predict the burning velocity in the premixed gas with water

83 vapor by the numerical simulation described in section 2.3.

84

85 *2.3. Numerical simulation of one-dimensional flame*

86 In order to validate the method for estimating the evaporation rate, we also conducted the numerical

87 simulation of the laminar flame. A one-dimensional flame was considered for prediction of the burning velocity

88 [31]. The premixed mixture was methane and air whose equivalence ratio was similarly 1.0. In the combustion

89 of diesel fuel, there are too many chemical reactions. Then, in the preliminary experiment, water was added in

90 the mixture, because it was much easier to take water into account in the combustion reaction. The reaction

91 mechanism for methane and air mixture was well-known, and GRI-Mech 3.0 [32] was adopted in the numerical

92 simulation with elementary reactions. When water was added in the premixed mixture, the burning velocity was

93 decreased. When the mass amount of water vapor was changed, the feeding rate of the water vapor to the flame

94 was also changed. The predicted burning velocity by the numerical simulation is shown in Fig. 5. Here, the

95 reduction of the burning velocity caused by the water vapor is ΔS_L, corresponding to the original burning of S_{L0}

96 subtracted of the decreased burning velocity of S_L caused by the water vapor. As seen in this figure, it is found

97 that ΔS_L is proportional to the feeding rate of the water vapor (dm_{H2O}/dt). Since the burning velocity can be

98 predicted by the simulation in advance by changing the amount of the added water, it is possible to estimate the

99 content of evaporated water from the porous ceramic tube in terms of the measured burning velocity.

Here, the one-dimensional flame is more explained. Since the spatial coordinate has only one, the upstream flow is unburned gas and the downstream flow is burned gas. The flame can be formed in the numerical domain if the flow velocity of the mixture is appropriate. In the simulation, the inflow velocity was adjusted to produce a stationary flame in the numerical domain, and the inflow velocity was naturally the laminar burning velocity of S_L. For the numerical domain, a 20-mm coordinate length was used. The number of numerical grids was 350. Around the region where the flame was formed, the spatial uniform grid of 0.02 mm was used. Irregular grids were adopted elsewhere. Similar to the experimental conditions, the temperature of the unburned gas was set to be 100°C, so that the water was gaseous water vapor in the simulation.

3. Results and discussion

3.1. Content of liquid impregnated in ceramic tube

111 Before we started the evaporation experiments, we needed to know aforehand the content of liquid

112 impregnated in the ceramic tube. The tube has hollow cylinder structure, and the thickness of the porous wall is

113 roughly 4 mm. The wall porosity of the ceramic tube is approximately 30%. To keep the experimental conditions

114 constant, it was desirable that the quantity of diesel fuel (or water) in the tube was constant. First, the container

115 filled with diesel fuel (or water) was prepared in which the porous ceramic tube was deeply doped, allowing it to

116 be filled with diesel fuel (or water). When the ceramic tube was taken out from the container, the quantity of

117 diesel fuel or water in the tube was measured using an electronic balance.

118 Figure 6 shows the mass change in water or diesel fuel in the porous ceramic tube. Table 1 shows the

119 quantity of water or diesel fuel impregnated in the tube up to 120 min after the filling was initiated. Figures 6 (a)

120 and (b) show the content of water or diesel fuel with filling time, respectively. The legend in these figures

121 corresponds to those of the experimental numbers in Table 1. Although each ceramic tube had different pore

diameter, length, and internal diameter (or external diameter), the content of water or diesel fuel was not changed after 120 min filling time. Moreover, the content differed according to their pore diameter, length, and internal diameter (or external diameter).

3.2. Measurement of evaporation rate by ELPI+

First, the amount of evaporated water was measured using the electrical low pressure impactor, ELPI+. The measurement was conducted for the porous ceramic tubes of experimental numbers, 1 to 3, which had a length of 100 mm and external diameter of 10 mm. By comparing the amount of water evaporated from these tubes, the effect of the pore diameter was investigated. In the experiments using water, the temperature of the tubular furnace was set to be 500°C, confirmed that the temperature of the mixture at the burner exit exceeded 100°C.

133 Figure 7 shows the particle number concentration, showing the temporal change in the number of

134 water droplets. As seen in Fig. 2, the sampling was conducted at the burner exit. Although the number

135 concentration rapidly increased after the experiment was started, it sometimes returned to nearly zero. Then, the

136 large fluctuation was repeatedly observed. Figure 8 shows the temporal change in the mass concentration of

137 water, which was calculated by the number and the sphere diameter of the water droplet. The mass evaporated

138 from the ceramic tube of 500 nm pore diameter was smaller than those of other two tubes.

139 The content of evaporated water was obtained using the measured mass concentration of water and

140 the flow rate by the following equation.

141 $$\frac{dm_{H2O}}{dt} = \sum C_{H2O} \times Q \quad (2)$$

142 Here, dm_{H2O}/dt is the evaporation rate of water, C_{H2O} (kg/m^3) is the mass concentration of water measured by

143 ELPI+ , and Q (m^3/s) is the flow rate of the mixture. Therefore, the total content of evaporated water from the

144 ceramic tube could be calculated by

145 $$m_{H2O} = \int_0^{T_{ev}} \frac{dm_{H2O}}{dt} dt \quad (3)$$

146 Here, T_{ev} represents the time when evaporation has completed, corresponding to the evaporation completion time.

147 The total contents of evaporated water were 20.8, 6.33, and 35.0 mg for 150, 500, and 1300 nm pore diameter

148 tubes. It should be noted that, as shown in Table 1, the mass of water initially impregnated in the tube were 1.45,

149 1.42, and 1.58 g, respectively. Therefore, the ratio of evaporated water measured using ELPI+ were only 1.43%,

150 0.45%, and 2.2%.

151 We tried to discuss the reason why the measured quantities of evaporated water was small. The

152 molecule size of water vapor is generally below 1 nm, but the lower limit of the particle size that can be measured

153 using ELPI+ is 6 nm. Therefore, ELPI+ could count liquid water droplets only, and could not measure the content

154 of gaseous water vapor. Conclusively, we conformed that most of evaporated water at the burner exit was water

155 vapor.

156

157 *3.3. Measurement of evaporation rate based on burning velocity*

158 In the previous section, it was revealed that ELPI+ could not successfully measure the amount of

159 gaseous evaporated water (water vapor). Then, we tested a new method based on the burning velocity. First, the

160 stationary flame was formed using the Bunsen burner, and the amount of evaporated water was estimated by the

161 change in the burning velocity caused by the water vapor from the ceramic tube. First, we discuss the effect of

162 water vapor on the flame shape. Flame photographs are shown in Fig. 9. Here, the porous ceramic tube of No. 4

163 (pore diameter: 1300 nm, length: 100 mm, external diameter: 12 mm) was used. One is the photograph of the

164 flame before the evaporation experiment. The other is that of the fluctuating flame with evaporated water. The

165 camera's exposure time was 4 s, and we recorded the flame shape at 5 s intervals. By comparing two photographs,

166 it was revealed that the height of the visible flame with vaporized water was slightly larger due to its smaller

167 burning velocity [33-35]. When water vaper is added in the mixture, there are three effects of a dilution effect

168 caused by the reduction in reactants concentration, a thermal effect due to the heat absorption of water vapor, and

169 a chemical effect in the combustion reaction [36]. It has been reported that the burning velocity is more reduced

170 when the concentration of water vapor is higher, finally causing the flame extinction.

171 Next, the temporal change in burning velocity before and after adding water was investigated. Results

172 are shown in Fig. 10. When the ceramic tube was placed at the flow line, the time was set to zero (t = 0 s). The

173 premixed gas was gradually preheated using the tubular furnace. To clarify the effect of adding water, we

174 measured the burning velocity using an empty porous ceramic tube (not filled with water), denoted as S_{L0}. As

175 seen in this figure, the burning velocity increased with time, and was constant approximately at t = 170 s. It was

176 the time when there was no water in the tube. The initial increase in the burning velocity was likely that the

177 temperature of the premixed gas was increased by the tubular furnace. When the tube filled with water was used,

178 the burning velocity started to decrease, but increased at t = 90 s and became constant approximately at t = 280

179 s. It looks reasonable, because adding water to the premixed gas has a negative effect of reducing the flame

180 temperature, resulting in a decrease in burning velocity. That is, water could weaken the combustion reaction,

181 even if there was the positive effect of the furnace by increasing the temperature. Resultantly, the burning velocity

182 showed the temporal change in Fig. 10.

183 Since we conducted the numerical simulation of the one-dimensional flame, it was possible to obtain

184 how much content of the vaporized water in the premixed gas. Here, ΔS_L is defined by the difference between

185 S_L and S_{L0}, corresponding to the effect of the vaporized water in the burning velocity. Based on the simulation, it

186 was revealed that the amount of water added to the premixed gas was proportional to ΔS_L. Then, we could

187 estimate the evaporation rate of dm_{H2O}/dt. Results are shown in Fig. 11 for porous ceramic tube of No. 4. It was

188 found that, when the ceramic tube was placed at the flow line, the evaporation rate increased due to the enlarged

189 temperature by the furnace. It took its maximum around $t = 100$ s, and gradually decreased to be zero at $t = 280$

190 s. This was because water impregnated in the porous ceramic tube had run out.

191

192 *3.4. Characteristics of ceramic tube based on fuel evaporation rate*

193 From the results of the preliminary experiments with water, it was confirmed that the evaporation rate

194 could be estimated based on the temporal change in burning velocity. Finally, the porous ceramic tubes filled

195 with diesel fuel were tested. The temperature of the tubular furnace was set to be 900°C. The temperature at the

196 burner exit was measured to be 230°C, ensuring that the evaporated diesel fuel from the ceramic tube did not

197 adhere to the pipe wall of the flow line. Figure 12 shows the flame photographs before and after adding diesel

198 fuel to the premixed gas. The camera's exposure time was 4 s. It was found that the flame length was longer

199 when the diesel fuel was evaporated. Since the diesel fuel was added, the equivalence ratio of the premixed gas

200 was more than 1.0. The premixed gas became fuel-rich, and consequently, the burning velocity decreased by the

201 evaporated diesel fuel, resulting in the larger flame height. In the case of fuel-rich condition, extra-fuel is the

202 additive which absorbs the heat of the stoichiometric mixture, resulting in the lower flame temperature. Moreover,

203 diesel fuel could affect the chemical reaction of methane-air flame.

204 Here, the effect of the pore size on the fuel evaporation rate was investigated. The temporal change in

205 burning velocity for tube numbers 1 to 3 are shown in Fig. 13. For all cases, the tube outer diameter was 10 mm,

206 and the tube length was 100 mm. As already defined, the burning velocities with and without evaporated diesel

207 fuel are denoted as S_{L0} and S_L, respectively. The temporal change in burning velocity in the diesel fuel experiments

208 was quite similar to those in the water experiments shown in Fig. 10. That is, when evaporated diesel fuel was

209 added to the premixed gas, the burning velocity decreased. When the diesel fuel in the ceramic tube completely

210 evaporated, the value of S_L finally became S_{L0}.

211 Next, the evaporation rate of diesel fuel (dm_f/dt) was estimated by the difference between S_L and S_{L0} in

212 Fig. 13. Figure 14 shows the evaporation rate for three cases of different pore diameters, 150, 500, and 1300 nm.

213 The maximum evaporation rate for 1300 nm pore size tube was higher than those of other two cases. Independent

214 of the pore size, the evaporation completion time was 230 s. Although it was difficult to conduct the numerical

215 simulation of the premixed flame with diesel fuel, the linearity between the amount of fuel and the reduction of

216 the burning velocity could not be shown. However, since the integrated value of the evaporated fuel shown in

217 Figs. 14 and 15 matched with the amount of fuel involved in the tube shown in Table 1, the validity of the

218 proposed method for estimating the fuel evaporation rate was confirmed.

219 Finally, effect of the tube length was investigated. Results are shown in Fig. 15. The tube lengths were

220 100, 200, and 280 mm, and the tube outer diameters were 10 and 12mm. For all cases, the pore size was 1300

221 nm. It should be noted that as the tube length was longer or the tube outer diameter was larger, more fuel was

222 impregnated in the ceramic tube. As for the effect of the tube length, it was found that the maximum evaporation

223 rate increased as the tube length was longer. It means that more fuel was evaporated. By comparing two figures,

224 it was revealed that the maximum evaporation rate increased when the tube diameter was larger. This could be

225 due to an increase in surface area of the fuel evaporation. However, the evaporation completion time was close

226 to 230 s regardless of the tube diameter.

227 In the case of the post fuel injection, it is reported that even the gaseous fuel is condensed near the

228 cylinder wall, and the liquid fuel reaches the cylinder wall and splashes away [37]. The typical droplet size is the

229 range of 5 to 10 micrometer. On the other hand, the size of the evaporated fuel or water from the nanopore-

230 ceramic tube was much smaller. It was the order of the vapor, because the measured mass of vaporized water in

231 Fig. 8 was much smaller than the amount of water in the tube. Although the uniformity of fuel distribution was

not confirmed in our experiments, our system supplies the gaseous fuel with more uniform fuel distribution, because the gaseous fuel flows and diffuses in the exhaust pipe to avoid condensed fuel region.

4. Conclusions

In this study, for the filter regeneration, we have tested an alternative fuel supply system to the DOC, where the fuel is uniformly vaporized on the surface of the nanopore-ceramic tube filled with the diesel fuel. Here, we measured the evaporation rate by the burning velocity of the premixed flame on the Bunsen burner, coupled with the electrical low pressure impactor, ELPI+. Following results were obtained.

(1) In the preliminary experiments with water, the ratio of evaporated water measured using ELPI+ were 1.43%, 0.45%, and 2.2% of the initial mass impregnated in the tube. The lower limit of particle size that could be

measured using ELPI+ was 6 nm, and it was much larger than the size of the water vapor molecule. Then, most of water vaporized from the ceramic tube was considered to be gaseous water vapor.

(2) When the premixed gas was preheated using the tubular furnace, the vaporized water was added to the premixed gas. The burning velocity firstly decreased and increased to become constant. This situation looks reasonable, because water in the premixed gas has the negative effect of reducing the flame temperature. Based on the temporal change of the burning velocity, it was revealed that the evaporation rate started to increase, took its maximum, and gradually decreased to be zero when water impregnated in the tube had run out.

(3) In the case of diesel fuel, the temporal change in burning velocity was quite similar to those in the water experiments. This is because when the evaporated diesel fuel was added to the premixed gas, the mixture became fuel-rich with the smaller burning velocity. The maximum evaporation rate of the tube whose pore

size was 1300 nm was larger than those of 150, 500 nm pore size. When the tube length or the tube outer diameter was larger, the fuel evaporation was enlarged due to the larger surface area of the fuel evaporation.

Acknowledgments

Nanopore-ceramic tubes needed for fuel supply system were presented by Noritake Co., Ltd. in Japan.

References

[1] https://unfccc.int/process-and-meetings/the-paris-agreement/the-paris-agreement.

[2] Zervas E, Poulopoulos S and Philippopoulos C. CO_2 emissions change from the introduction of diesel passenger cars: Case of Greece. Energy 2006; 31:2579-89.

[3] Knecht W. Diesel engine development in view of reduced emission standards. Energy 2008; 33:264-71.

[4] Johnson JE and Kittelson DB. Deposition, diffusion, and adsorption in the diesel oxidation catalyst. Applied Catalysis B: Environmental 1996; 10:117-37.

[5] Kennedy IM. The health effects of combustion-generated aerosols. Proc. Combust. Inst 2007; 31:2757-70.

[6] Johnson TV. Vehicular emissions in review. SAE Int. J. Engines 2016; 9:1258-75.

[7] Winkler SL, Anderson JE, Garza L, Ruona WC, Vogt R, Wallington TJ. Vehicle criteria pollutant (PM, NOx, CO, HCs) emissions: how low should we go? Climate and Atmospheric Science 2018; 26:1-5.

[8] Schejbal M, Šteˇpánek J, Marek M, Kocˇí P, Kubícˇek M. Modelling of soot oxidation by NO_2 in various types of diesel particulate filters. Fuel 2010; 89:2365-75.

[9] Tsuneyoshi K, Takagi O, Yamamoto K. Effects of washcoat on initial PM filtration efficiency and pressure drop in SiC DPF. SAE Technical Paper 2011; 2011-01-0817:1-10.

[10] Lapuerta M, Oliva F, Agudelo JR, Boehman AL. Effect of fuel on the soot nanostructure and consequences on loading and regeneration of diesel particulate filters. Combust Flame 2012; 159:844-53.

[11] Tsuneyoshi K, Yamamoto K. Experimental study of hexagonal and square diesel particulate filters under controlled and uncontrolled catalyzed regeneration. Energy 2013; 60:325-32.

[12] Gong J, Viswanathan, S, Rothamer SA, Foster DA, Rutland CJ. Dynamic heterogeneous multiscale filtration model: probing microand macroscopic filtration characteristics of gasoline particulate filters. Environ. Sci. Technol 2017; 51:11196-204.

281 [13] Czerwinski J, Comte P, Heeb N, Mayer A, Hensel V. Nanoparticle emissions of DI gasoline cars
282 with/without GPF. SAE Technical Paper 2017; 2017-01-1004:1-8.
283 [14] Jang J, Lee J, Choi Y, Park S. Reduction of particle emissions from gasoline vehicles with direct fuel injection
284 systems using a gasoline particulate filter. Sci. Total Environ 2018; 644:28-33.
285 [15] Yamamoto K, Kondo S, Suzuki K. Filtration and regeneration performances of SiC fiber potentially applied
286 to gasoline particulates. Fuel 2019; 243:28-33.
287 [16] Yamamoto K, Kanamori Y. Measurements of size distribution and oxidation rate of PM with NO_2. SAE
288 Technical Paper 2015; 2015-01-1995:1-7.
289 [17] Yamamoto K, Sakai T. Simulation of continuously regenerating trap with catalyzed DPF. Catalysis Today
290 2015; 242:357-62.
291 [18] Kong H, Yamamoto K, Simulation on soot deposition in in-wall and on-wall catalyzed diesel particulate

292 filters. Catalysis Today 2019; 332:89-93.

293 [19] Yamamoto K, Yamauchi K. Numerical simulation of continuously regenerating diesel particulate filter. Proc.

294 Combust. Inst., 2013; 34:3083-90.

295 [20] Abián M, Martín C, Nogueras P, S-Valdepeñas S, R-Fernández J, Lapuerta M, Alzueta MU. Interaction of

296 diesel engine soot with NO_2 and O_2 at diesel exhaust conditions. Effect of fuel and engine operation mode.

297 Fuel 2018; 242:455-61.

298 [21] Yamamoto K, Komiyama R, Sakai T. Flow and pressure variations through porous filter during soot

299 filtration and regeneration. ASME J. Thermal Sci. Eng. Applications 2019; 1:1-7.

300 [22] Zuo Q, Zhu X, Zhang, J, Zhang B, Tang Y, Xie Y, Zhang X, Zhu G, Wang Z. Effects of exhaust parameters

301 on temperature and pressure drop of the gasoline particulate filter in the regeneration equilibrium state. Fuel

302 2019; 257:1-10.

303 [23] Desantes JM, Bermúdez V, Pastor JV, Fuentes E. Investigation of the influence of post-injection on diesel
304 exhaust aerosol particle size distributions. Aerosol Science and Technology 2006; 40:80–96.
305 [24] O'Connor J, Musculus M. Post injections for soot reduction in diesel engines: a review of current
306 understanding. SAE Technical Paper 2013; 2013-01-0917:1-22.
307 [25] Abdalla A, Wang G, Zhang J, Shuai SJ. Simulation of catalyzed diesel particulate filter for active
308 regeneration process using secondary fuel injection. SAE Technical Paper 2017; 2017-01-2287:1-14.
309 [26] Kaniyu J, Sakatani S, Matsumura E, Kitamura T. Analysis of spray feature injected by tailpipe injector for
310 aftertreatment of diesel engine emissions. SAE Technical Paper 2017; 2017-01-2373:1-11.
311 [27] Cizeron JM, Betta RAD. Pre-combustors for internal combustion engines and systems and methods
312 therefor. US Patent 2007; 7,240,483 (Navistar), https://patents.google.com/patent/US7240483B2.
313 [28] Hein E, Kotrba A, Inclan T, Bright A. Secondary fuel injection characterization of a diesel vaporizer for

active DPF regeneration. SAE Int. J. Engines 2014; 7:1228-34.

[29] Järvinen A, Aitomaa M, Rostedt A, Keskinen J, Yli-Ojanperä Y. Calibration of the new electrical low pressure impactor (ELPI+). J Aerosol Sci 2014; 69:150-59.

[30] Cornette JFP, Coppieters T, Desagher D, Annendijck J, Lepaumier H, Faniel N, Dyakov I, Blondeau J, Bram S. Influence of the dilution system and electrical low pressure impactor performance on particulate emission measurements from a medium-scale biomass boiler. J Aerosol and Air Quality Research 2020; 20:499-519.

[31] Yamamoto K, Ozeki M, Hayashi N, Yamashita H. Burning velocity and OH concentration in premixed combustion. Proc Combust Inst 2009; 32:1227-1235.

[32] GRI-Mech, http://www.me.berkley.edu/gri_mech.

[33] Babkin VS, V'yun AV. Effect of water vapor on the normal burning velocity of a methane-air mixture at high pressures. Combust Explosion and Shock Waves 1971; 7:339–341.

325 [34] D.D.S. Liu DDS, MacFarlane R. Laminar burning velocities of hydrogen-air and hydrogen-air-steam
326 flames. Combust Flame; 1983; 49:59-71.
327 [35] Koroll GW, Mulpuru SR. The effect of dilution with steam on the burning velocity and structure of premixed
328 hydrogen flames. Proc Combust Inst 1988; 21:1811-1819.
329 [36] Mazas AN, Fiorina B, Lacoste DA, Schuller T. Effects of water vapor addition on the laminar burning
330 velocity of oxygen-enriched methane flames. Combust Flame; 2011; 158:2428-2440.
331 [37] Shibata G, Nishiuchi S, Takai S, Kobashi Y, Kanbe H, Matsumura E. Fuel adhesion and oil splash on oil-
332 wet cylinder walls with post diesel fuel injections. Int. J. Engine Research 2020;
333 https://doi.org/10.1177/1468087420914142.
334

335 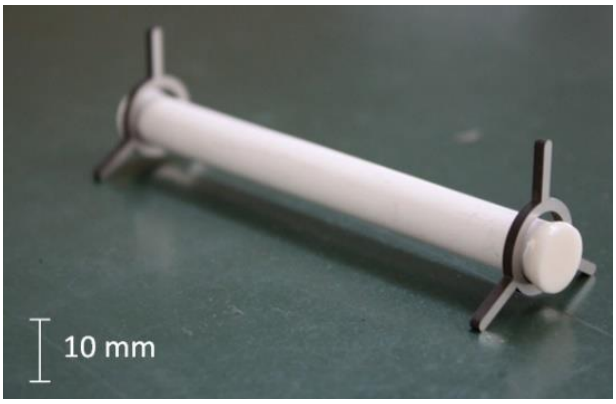

336 Fig.1 Nonopore-ceramic tube

337

338 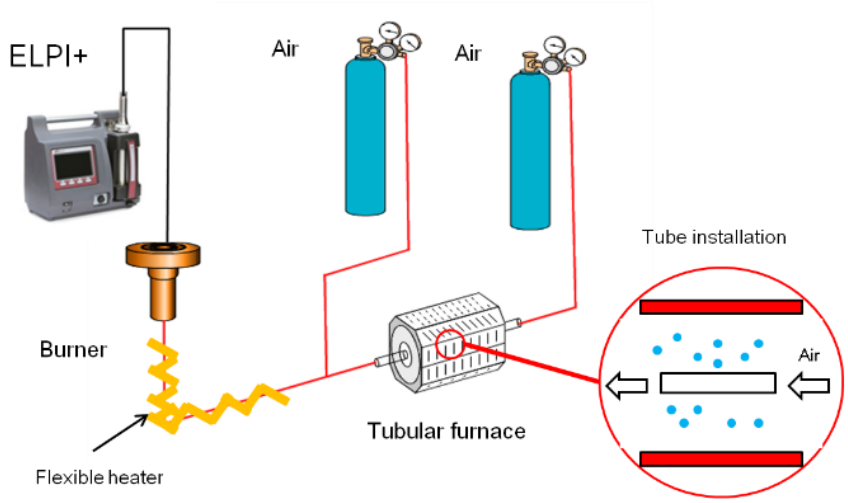

339 Fig. 2 Experimental setup using ELPI+

340

341

342

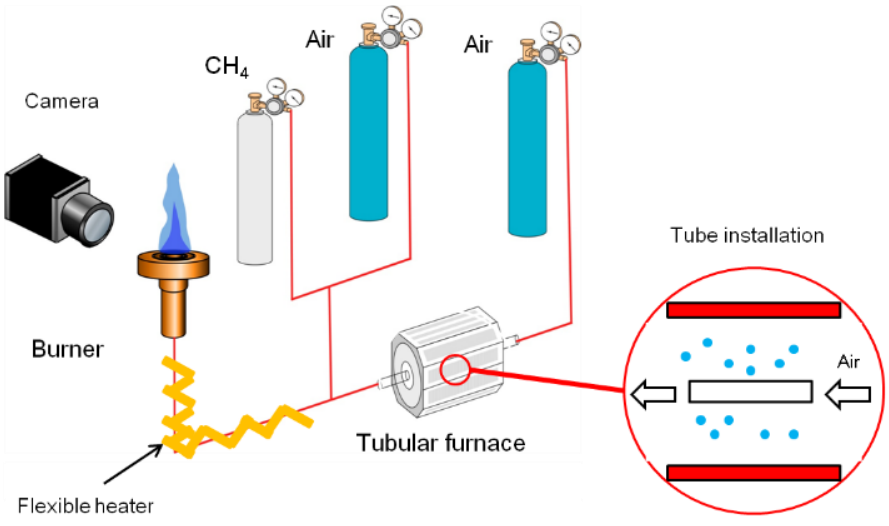

343

344 Fig. 3 Experimental setup using a premixed flame

345

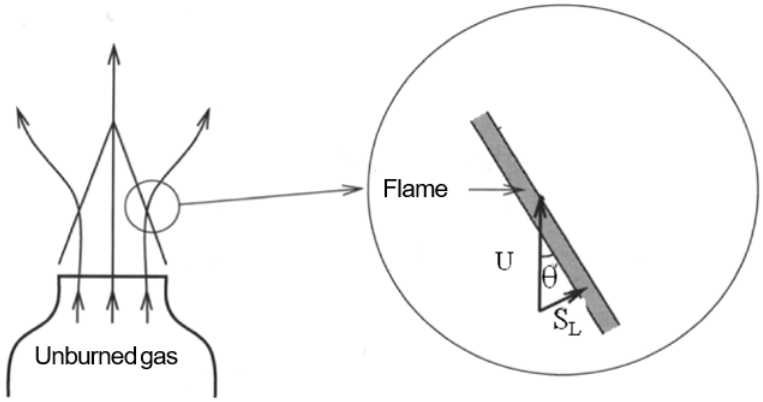

346

347 Fig. 4 Flame shape and burning velocity

348

349

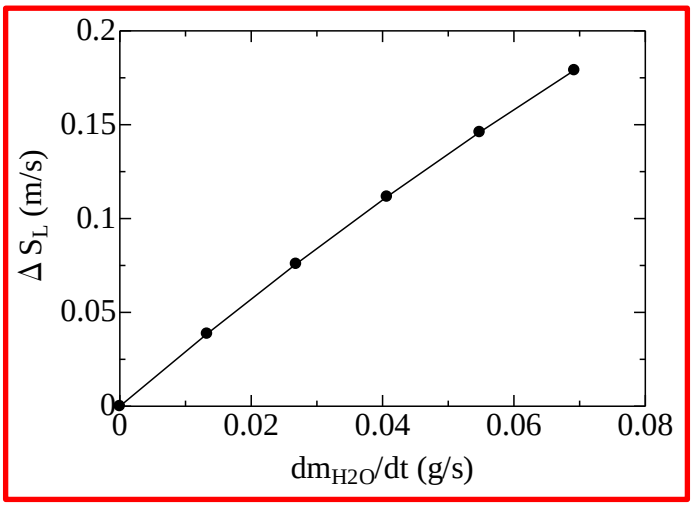

Fig. 5 Relationship between the feeding rate of the water vapor and the reduction of the predicted burning velocity caused by the water vapor

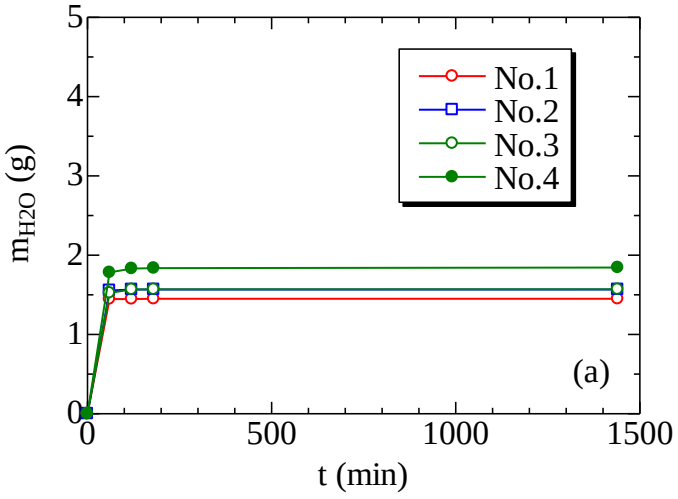

360

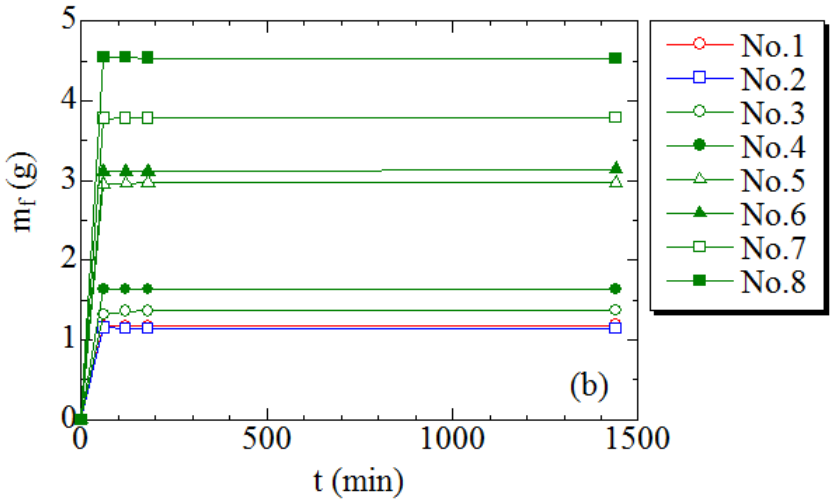

361

362 Fig. 6 Mass in porous ceramic tube filled with (a) water and (b) diesel fuel

363

364

365

366 Table 1 Mass in porous ceramic tube filled with water and diesel fuel

No.	Pore size [nm]	Length [mm]	I.D. [mm]	O.D [mm]	Water [g]	Diesel oil [g]
1	150	100	6.9	10	1.4470	1.1796
2	500	100	6.9	10	1.5661	1.1409
3	1300	100	6.9	10	1.5678	1.3607
4	1300	100	9.0	12	1.8308	1.6333
5	1300	200	6.9	10	-	2.9606
6	1300	200	9.0	12	-	3.1181
7	1300	280	6.9	10	-	3.7803
8	1300	280	9.0	12	-	3.7614

367

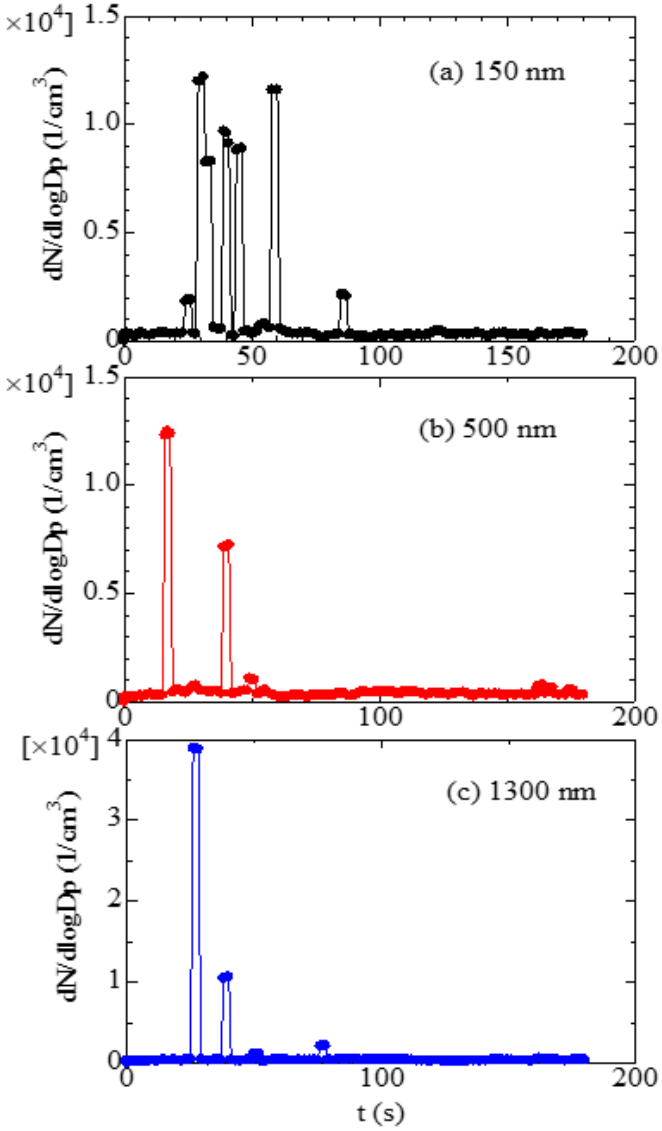

368

369 Fig. 7 Particle number concentration

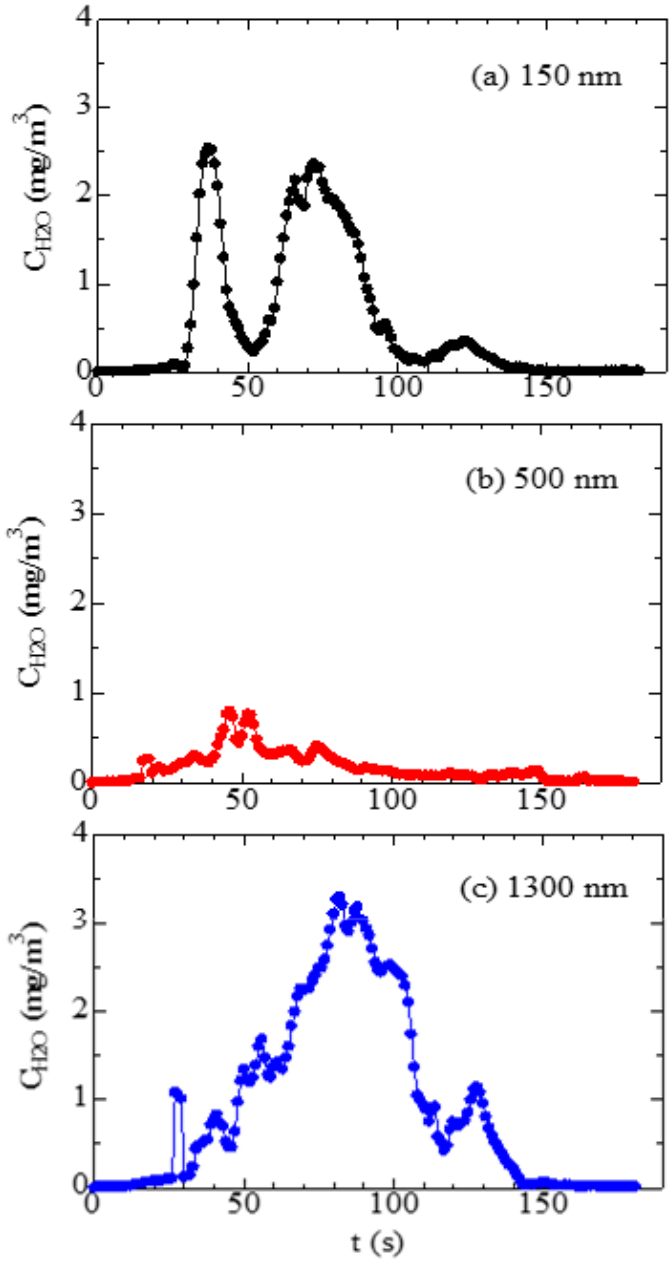

370

371 Fig. 8 Particle mass concentration

372

373 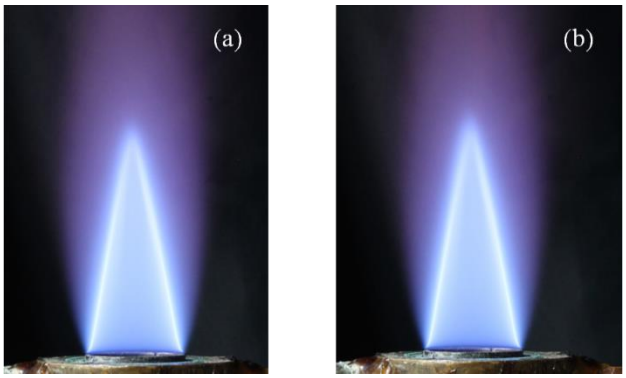

374 Fig. 9 Photographs of flames (a) without vaporized water, (b) with vaporized water

375

376 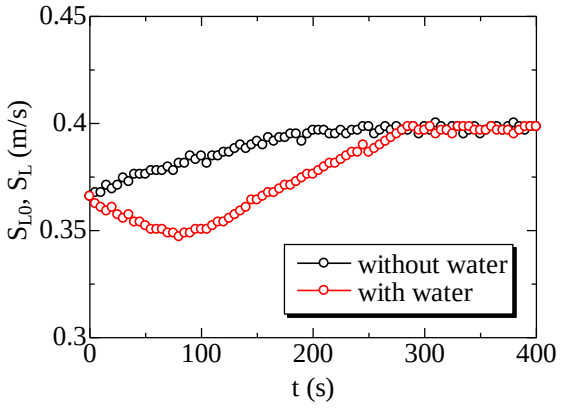

377 Fig. 10 Burning velocity with and without water

378

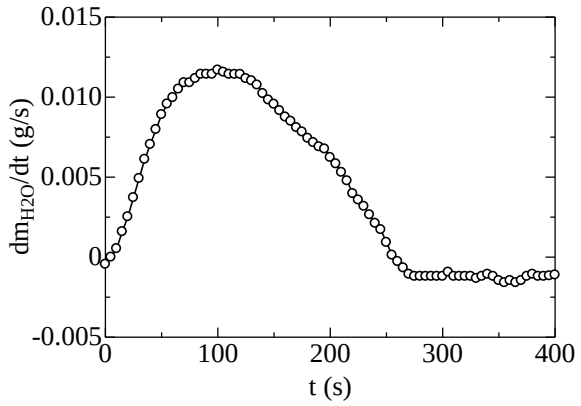

379

380 Fig. 11 Evaporation rate of water

381

382

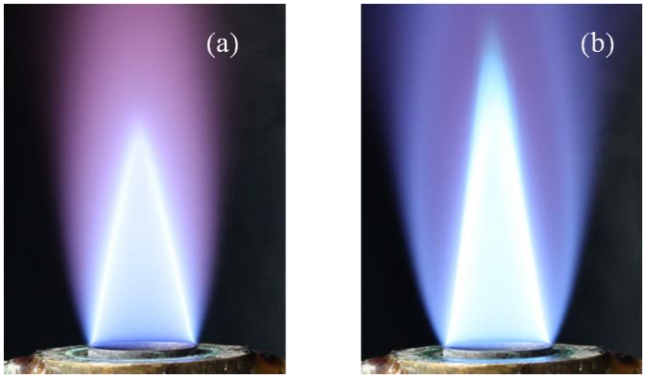

383

384 Fig. 12 Photographs of flames; (a) without fuel, (b) with fuel

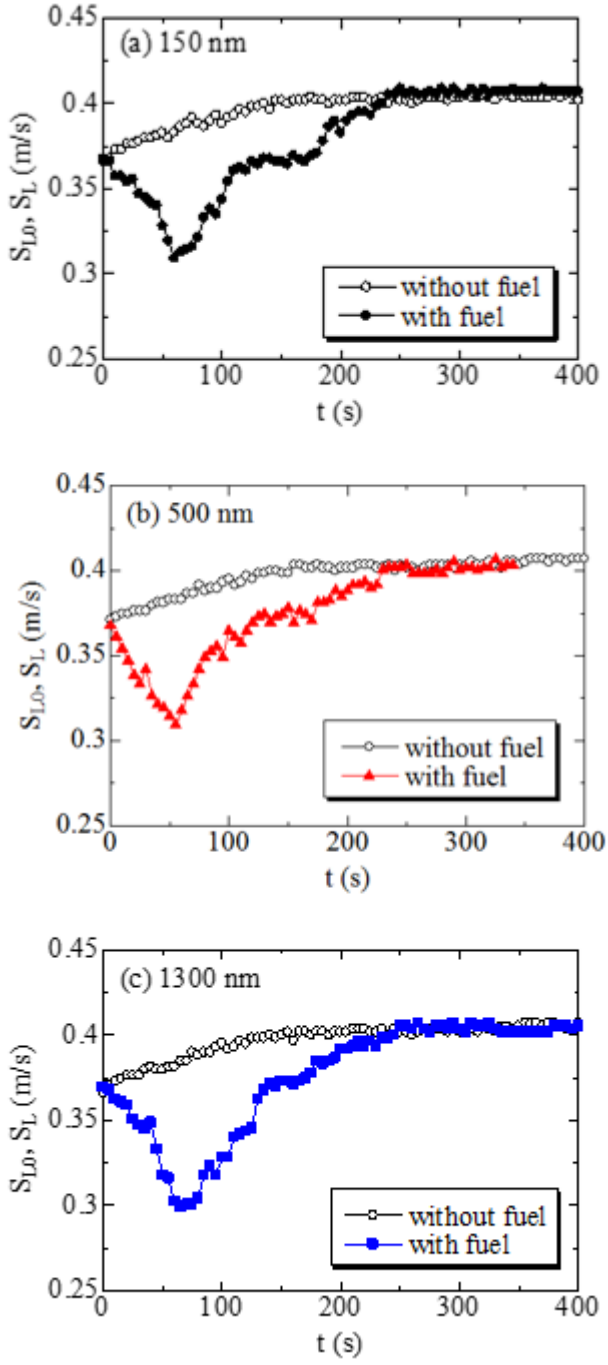

385

386 Fig. 13 Burning velocity of (a)150 nm, (b)500 nm, (c)1300 nm

387

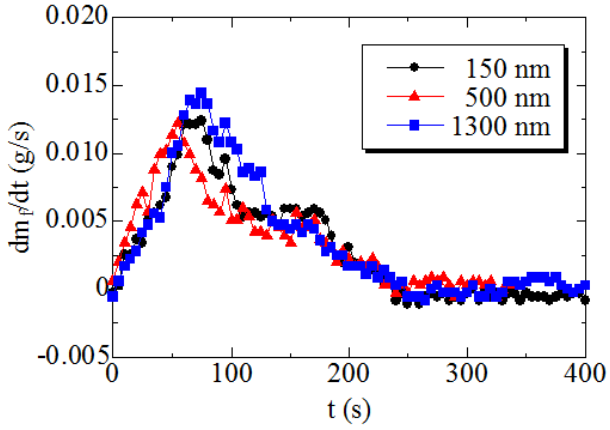

388

389 Fig. 14 Evaporation rate of diesel fuel

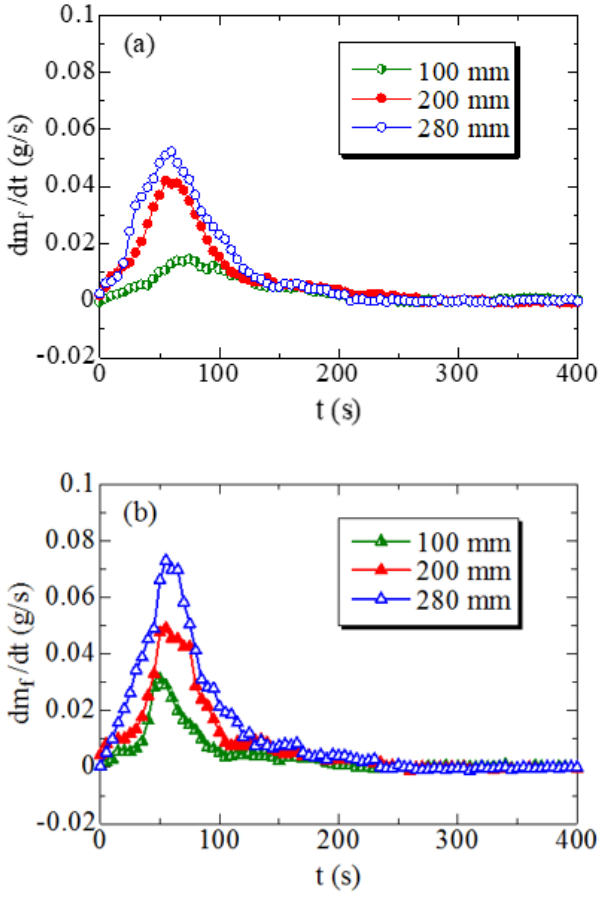

390

391 Fig. 15 Fuel evaporation rate of (a) 10 mm, (b) 12 mm